A Comparison of Techniques for Coupling Porous Flow and Geomechanics

R.H. Dean, SPE, Simwulf Systems; **X. Gai,** U. of Texas at Austin; **C.M. Stone,** Sandia Natl. Laboratories; and **S.E. Minkoff,** U. of Maryland, Baltimore County

Summary

This paper compares three techniques for coupling multiphase porous flow and geomechanics. Sample simulations are presented to highlight the similarities and differences in the techniques. One technique uses an explicit algorithm to couple porous flow and displacements in which flow calculations are performed every timestep and displacements are calculated only during selected timesteps. A second technique uses an iteratively coupled algorithm in which flow calculations and displacement calculations are performed sequentially for the nonlinear iterations during each timestep. The third technique uses a fully coupled approach in which the program's linear solver must solve simultaneously for fluid-flow variables and displacement variables. The techniques for coupling porous flow with displacements are described and comparison problems are presented for single-phase and three-phase flow problems involving poroelastic deformations. All problems in this paper are described in detail, so the results presented here may be used for comparison with other geomechanical/porous-flow simulators.

Introduction

Many applications in the petroleum industry require both an understanding of the porous flow of reservoir fluids and an understanding of reservoir stresses and displacements. Examples of such processes include subsidence, compaction drive, wellbore stability, sand production, cavity generation, high-pressure breakdown, well surging, thermal fracturing, fault activation, and reservoir failure involving pore collapse or solids disposal. It would be useful to compare porous flow/geomechanics techniques for all of these processes, because some of these processes involve a stronger coupling between porous flow and geomechanics than others. However, this paper looks at a subset of these processes and compares three coupling techniques for problems involving subsidence and compaction drive. All of the sample problems presented in this paper assume that the reservoir absolute permeabilities are constant during a run. Displacements influence fluid flow through the calculation of pore volumes, and fluid pressures enter the displacement calculations through the poroelastic constitutive equations.

Several authors have presented formulations for modeling poroelastic, multiphase flow. Settari and Walters (1999) discuss the different methods that have been used to combine poroelastic calculations with porous flow calculations. They categorize these different methods of coupling poroelastic calculations with porous flow calculations as decoupled (Minkoff *et al.* 1999a), explicitly coupled, iteratively coupled, and fully coupled. The techniques discussed in this paper are explicitly coupled, iteratively coupled, and fully coupled.

For an explicitly coupled approach (Settari and Walters 1999; Minkoff *et al.* 1999b; Minkoff *et al.* 2003), a simulator performs computations for multiphase porous flow each timestep and performs geomechanical calculations for displacements during selected timesteps. The frequency of geomechanical updates is driven by the magnitude of the pore-volume changes during the timesteps. If the pore volumes change slowly during timesteps, then few geomechanical updates are required. The ability to perform geomechanical calculations for selected timesteps is a very attractive feature of the explicitly coupled approach because a major portion of the computational time for a porous-flow/geomechanics run is often spent in calculating displacements. Another attractive feature of the explicitly coupled approach is that it is very straightforward to use this technique to couple an existing porous-flow simulator with an existing geomechanics simulator. One shortcoming of the explicitly coupled approach is that the explicit nature of the coupling can impose timestep restrictions on runs because of concerns about stability and accuracy. However, for many subsidence problems, the fluid-flow calculations require timesteps that are smaller than those imposed by the explicit coupling calculations.

For the iteratively coupled approach, multiphase porous flow and displacements are coupled through the nonlinear iterations for each timestep. During each nonlinear iteration, a simulator performs computations sequentially for multiphase porous flow and for displacements. The flow and displacement calculations are then coupled through calculations of pore volumes at the end of each nonlinear iteration. An iteratively coupled approach will produce the same results as a fully coupled approach if both techniques use sufficiently tight convergence tolerances for iterations. Settari and Mourits (1994) and Fung *et al.* (1994) present examples of the iteratively coupled approach for multiphase flow. The primary attraction of the iteratively coupled approach is that it is very straightforward to couple an existing porous-flow simulator with an existing geomechanics simulator. The primary drawback to the iteratively coupled approach is that the calculations may display a first-order convergence rate in the nonlinear iterations; therefore, it may require a large number of iterations for difficult problems.

For the fully coupled approach, porous-flow and displacement calculations are performed together, and the program's linear solver must handle both fluid-flow variables and displacement variables. Tortike and Farouq Ali (1987), Li and Zienkiewicz (1992), and Lewis and Sukirman (1993) have presented formulations of the fully coupled approach for poroelastic, multiphase flow. The primary attraction of the fully coupled approach is that it is the most stable approach of the three techniques and preserves second-order convergence of nonlinear iterations. Drawbacks to the fully coupled approach include the following: it may be difficult to couple existing porous-flow simulators and geomechanics simulators, it requires more code development than other techniques, and it can be slower than the explicit and iterative techniques on some problems.

The three techniques for coupling porous flow and geomechanics were incorporated into the same program so that differences in the calculations could be attributed to the different techniques for coupling. If one were to compare three different programs, each using a different technique for coupling, then it might be difficult to differentiate between differences caused by coupling and differences caused by basic algorithms in the separate programs. Comparison problems are presented for single-phase and three-phase flow problems involving poroelastic deformations. All techniques should produce the same results when using small timesteps and tight convergence tolerances, so the choice between techniques is determined by ease of implementation, program availability, numerical stability, and computational efficiency.

A short review of the equations coupling porous flow and deformations is presented, followed by details of the algorithm for

This paper (SPE 79709) was first presented at the 2003 SPE Reservoir Simulation Symposium, Houston, 3–5 February, and revised for publication. Original manuscript received for review 3 February 2003. Revised manuscript received 25 November 2005. Paper peer approved 29 November 2005.

explicit coupling. Four problems are then presented, and the results are compared using the three techniques. The first two problems are simple single-phase depletion problems that illustrate the role that stress and displacement boundary conditions play in porous-flow calculations. The third problem is a single-phase depletion example in which a soft reservoir is contained within a stiff nonpay region. The final problem is a three-phase, black-oil, five-spot pattern with a production well in one corner of the grid and a water-injection well in the opposite corner. The coupling between geomechanics and fluid flow is fairly straightforward in Problems 1, 2, and 4, and pressure histories for these runs can be reproduced by typical reservoir simulators with proper choices of compressibilities; however, Problem 3 exhibits geomechanical effects that cannot be seen in reservoir simulations that do not include geomechanical calculations.

Coupled Flow and Deformation

For the problems in this paper, displacements enter the fluid-flow equations through the calculation of reservoir pore volumes, and fluid pressures enter the displacement calculations through the stress/strain constitutive equations. A typical porous-flow simulator expresses the pore volume for a gridblock as

$$V_p = V_p^o[1 + c_r(p - p_o)], \quad \ldots\ldots\ldots\ldots\ldots\ldots\ldots\ldots (1)$$

where p is the fluid pressure and c_r is a compressibility term that must be entered by the user as part of the input data. For linear poroelastic calculations, the pore volume for infinitesimal displacements may be expressed as

$$V_p = V_b^o\left[\varphi_o + \alpha\varepsilon_{kk} + \frac{1}{M}(p - p_o)\right], \quad \ldots\ldots\ldots\ldots\ldots\ldots\ldots\ldots (2)$$

where α and $1/M$ are Biot's parameters (1956), expansion is positive, and summation over k is implied for the bulk volumetric strain ε_{kk}. The term V_b^o is the initial bulk volume and the pore volume at $\varepsilon_{kk} = 0$, and $p = p_o$ is $V_b^o\,\varphi_o$. Eq. 2 follows directly from Biot's Eq. 25, where the change in pore volume for Eq. 2 corresponds to the change in fluid content in Biot's Eq. 25. For the comparisons in this paper, α and $1/M$ are set equal to one and zero, respectively. For this choice of Biot's parameters, Eq. 1, a typical equation for flow simulators, expresses the pore volume in terms of the fluid pressure, while Eq. 2 expresses the pore volume in terms of bulk strains, ε_{kk}. Flow simulators that are coupled to geomechanics programs may use an equation similar to Eq. 1 to approximate pore volume changes for the flow calculations and use an equation similar to Eq. 2 to calculate corrected pore volumes based upon reservoir deformations.

Logic that couples flow simulators to geomechanics programs must somehow account for the discrepancies between Eqs. 1 and 2. Many coupling techniques will normally use a c_r term similar to that in Eq. 1 to enhance the coupling between flow calculations and displacement calculations. For explicitly coupled techniques, modified forms of Eq. 1 may be used to calculate pore volumes for those timesteps where geomechanical updates are not performed. For iteratively coupled techniques, a c_r term may be included in the Jacobian for the flow equations, but Eq. 2 is always used to calculate pore volumes. For fully coupled techniques, a c_r term may be used in a preconditioning matrix for the flow equations when solving the linear system for flow variables and displacement variables.

The fluid pressure enters the deformation calculations through the linear poroelastic constitutive equation

$$\sigma_{ij} = \sigma_{ij}^o + \lambda\varepsilon_{kk}\delta_{ij} + 2\mu\varepsilon_{ij} - \alpha(p - p_o)\delta_{ij}, \quad \ldots\ldots\ldots\ldots\ldots\ldots (3)$$

where tensile stresses are positive in Eq. 3. For the three-phase simulation included in this paper, the oil-phase pressure is used in Eqs. 1 through 3. For explicitly coupled and iteratively coupled techniques, the fluid pressure in Eq. 3 may be included in the equilibrium equation as a forcing function similar to the effects of a gravity head term. For a fully coupled technique, the fluid pressure in Eq. 3 generates coefficients that must be included in the Jacobian for the system of flow variables and displacement variables.

Explicit Coupling

The coupling algorithm for the explicit technique is described in more detail here because the algorithm uses both Eq. 2 and a modified form of Eq. 1 to calculate pore volumes for gridblocks during simulations. The iteratively coupled and fully coupled techniques may use a c_r term for the Jacobian or in a preconditioner to accelerate iterative calculations, but never actually use Eq. 1 to calculate pore volumes.

The explicit coupling algorithm allows a program to perform geomechanical calculations on a time scale that is different from the time scale for the flow calculations. This is very useful for subsidence problems because a large portion of the computational time in a simulation can be spent in performing geomechanical calculations. For many problems, fluid fronts may propagate or well changes may occur over very short time frames, while subsidence may progress very slowly throughout the course of a simulation.

One can use Eqs. 1 and 2 to develop an algorithm for determining how often geomechanical calculations must be performed during a simulation. Let V_p^m be the pore volume for a gridblock at timestep m that was calculated using the geomechanical expression in Eq. 2. If the last geomechanical calculation was done for timestep m, then for timestep $n>m$, the pore volume in a gridblock may be approximated by

$$\tilde{V}_p^n = V_p^m + c_r^{\text{est}} V_p^o (p^n - p^m), \quad \ldots\ldots\ldots\ldots\ldots\ldots\ldots (4)$$

where p^n and p^m are the pressures for the gridblock at timesteps n and m, respectively. One may replace the V_p^o term in Eq. 4 by V_p^m; however, this does not change the accuracy of the approximation, because terms at step m are constant in Eq. 4. Using V_p^m in place of V_p^o merely modifies the formula that one would develop for estimating values for the compressibility, c_r^{est}, at step m. Several techniques may be used to estimate compressibilities during a simulation. One approach derives analytical estimates of compressibilities using simple assumptions concerning stress and strain variations for a problem, while a second approach uses pressure and pore volume changes between previous geomechanical updates during a simulation to estimate compressibilities. A third approach might calculate numerical estimates from the geomechanical equilibrium equations by calculating how variations in fluid pressures affect displacements. When estimating compressibilities, one may need to establish bounds for these estimates, because values that are too large generate significant numerical errors, and values that are too small give rise to oscillations or instabilities.

The explicitly coupled simulations in this paper use compressibilities in Eq. 4 that are derived from simple assumptions concerning stress and strain variations. For example, when a reservoir is deforming in the vertical direction and horizontal displacements are zero, uniaxial strain, then Eqs. 2 and 3 become approximately $\Delta V_p = V_b^o \Delta\varepsilon_{zz}$ and $\Delta\varepsilon_{zz} = \Delta p/(\lambda+2\mu)$ when $\alpha = 1$ and $1/M = 0$. Therefore, Eqs. 2 and 3 may be combined as $\Delta V_p = V_b^o \Delta p/(\lambda+2\mu)$. But Eq. 4 may be written as $\Delta\tilde{V}_p^n = c_r^{\text{est}} \varphi_o V_b^o \Delta p$, which produces an estimate for c_r^{est} that is $[(\lambda+2\mu)\varphi_o]^{-1}$. This may also be written in terms of the elastic modulus and Poisson's ratio as $(1+\nu)(1-2\nu)/[1-\nu)\varphi_o E]$.

If one uses the geomechanical expression in Eq. 2 to calculate the pore volume V_p^n at step n, then one can compare V_p^n with $\tilde{V}_p^n$ to determine errors in using Eq. 4 in place of Eq. 2. The relative error in pore volume for step n may be written as

$$E_{\text{rel}} = \text{abs}\left(\frac{\tilde{V}_p^n - V_p^n}{V_p^n}\right). \quad \ldots\ldots\ldots\ldots\ldots\ldots\ldots\ldots (5)$$

During an explicitly coupled simulation, one does not have a value of E_{rel} for every timestep, but only for those steps at which geomechanical calculations are performed. It is natural to assume that the error in Eq. 5 is related to the relative change in pore

volume since the last geomechanical update at step m, where the relative change in pore volume between steps m and n is approximated by

$$(\Delta V_p)_{\text{rel}} = \text{abs}\left(\frac{\tilde{V}_p^n - V_p^m}{V_p^m}\right). \quad \ldots\ldots\ldots\ldots\ldots\ldots\ldots\ldots (6)$$

If one assumes that E_{rel} is proportional to $(\Delta V_p)_{\text{rel}}$ for those timesteps where geomechanical calculations are not performed, then one can implement an algorithm that determines when displacements must be updated. One may estimate the parameter β in $E_{\text{rel}} \approx \beta(\Delta V_p)_{\text{rel}}$ as

$$\beta = \frac{E_{\text{rel}}}{(\Delta V_p)_{\text{rel}}}, \quad \ldots\ldots\ldots\ldots\ldots\ldots\ldots\ldots\ldots\ldots\ldots\ldots (7)$$

where values of E_{rel} and $(\Delta V_p)_{\text{rel}}$ are determined from the two most recent timesteps that included geomechanical updates. Prescribing a tolerance for E_{rel}, one may then use $\beta(\Delta V_p)_{\text{rel}}$ to determine when geomechanical updates need to be performed during subsequent timesteps. The algorithm presented here is concerned with errors in pore volumes; however, similar logic may be applied to permeabilities if permeabilities change during a simulation. For the problems in this paper, the tolerance for E_{rel} is set to 0.001. The program also has options to specify updates for displacements after a prescribed number of timesteps or after a prescribed pressure change since the last update, but neither option was used for the problems in this paper.

Program Description

The three techniques for coupling flow and geomechanics are available in the program ACRES (ARCO's Comprehensive REservoir Simulator)(1999). The program uses masses and a fluid pressure as primary variables for the flow equations and displacements as primary variables for deformations. The program contains IMPEM (IMplicit Pressure Explicit Mass) and implicit timestepping algorithms; however, all coupled runs are restricted to using the IMPEM technique for the flow calculations.

ACRES was originally developed for general porous-flow applications and uses finite differences (mixed finite elements on rectangular prisms with piecewise constant pressures) for the flow variables. The program was used throughout ARCO to model full-field, porous-flow applications involving both black-oil and fully compositional processes. Geomechanical capabilities were added to the program later for multiphase, porous-flow applications involving subsidence and solid-waste disposal.

Originally, a finite-difference method was implemented for the deformation equations, and the equations were then coupled with the porous-flow equations. However, the linear system is singular for standard finite-difference implementations of the deformation equations. The nonuniqueness arises because there are hourglass-type deformations that produce zero energy for the system of finite-difference equations. The singularities can be removed from the system of finite-difference equations by appropriate application of damping terms (Maenchen and Sack 1964). One can also implement finite-element algorithms that use single-point integration, and these schemes are similar to a finite-difference method. However, these single-point finite-element schemes also require damping techniques for hourglass control (Kosloff and Frazier 1978; Belylschko *et al.* 1984). In order to avoid damping algorithms in the deformation equations, a standard finite-element technique for hexahedra with eight Gaussian integration nodes was implemented for the deformation equations.

The current version of the program evaluates masses and fluid pressure at the center of each element and displacements are evaluated at the corners of each element. Trilinear basis functions are used to approximate the displacements throughout each element. Eight Gaussian integration nodes are used to form the stiffness matrix, and a single integration node at the center of each element is used to integrate the fluid pressure in the equilibrium equation. The program is capable of performing poroelastic and poroplastic calculations for black-oil and fully compositional applications.

Comparison Problems

Four problems are used to compare the three techniques for coupling porous flow and geomechanics. The first two problems are simple single-phase depletion problems that illustrate the role that stress and displacement boundary conditions play in porous-flow calculations. The third problem is a single-phase depletion example in which a soft reservoir is contained within a stiff nonpay region. The final problem is a three-phase, black-oil, five-spot pattern with a production well in one corner of the grid and a water-injection well in the opposite corner. Biot's parameters α and $1/M$ are set equal to one and zero, respectively, for all problems. All stresses described are compressive and represent total stresses for the systems (include forces for fluid and solid).

All problems in this paper use a nonlinear convergence tolerance of 0.01 for volume errors and a relative residual reduction tolerance of 0.01 for linear iterations, unless stated otherwise. The volume error is expressed as $(V_f - V_p)/V_p$ and the maximum is calculated for all gridblocks, where V_f and V_p are the fluid and pore volumes for a cell, respectively. All computing times presented in this paper are for a 700 Mhz Intel Mobile Pentium III.

Problems 1 and 2. Problems 1 and 2 are identical in description, with the exception that Problem 1 enforces zero displacement boundary conditions at the vertical faces of the grid, while Problem 2 applies constant horizontal stresses at the vertical faces of the grid. **Figs. 1a and 1b** show the stress and displacement boundary conditions for the two problems.

The grid is 11×11×10 with $\Delta x = \Delta y = 200$ ft in the horizontal directions and $\Delta z = 20$ ft in the vertical direction. The top of the grid is at a depth of 6,000 ft; the initial in-situ reservoir porosity is 20%; and the reservoir permeabilities are 50 and 5 md in the horizontal and vertical directions, respectively. The fluid is single-phase, with a formation volume factor of 1.0, a viscosity of 1 cp, a fluid density of 62.4 lbm/ft^3, and zero fluid compressibility. The initial fluid pressure is 3,000 psi at a depth of 6,000 ft and has a vertical hydrostatic gradient of 0.433 psi/ft.

The elastic modulus is 1×10^4 psi, Poisson's ratio is 0.3, and the initial in-situ solid density (solid material without pores) is 2.7 g/cm^3. Initial horizontal stresses are 4,000 psi over the entire reservoir depth, while the initial vertical stress is 6,000 psi at 6,000 ft with a vertical stress gradient of 1.0231 psi/ft throughout the reservoir. The bottom of the grid has a zero vertical displacement constraint and all faces of the grid have zero tangential stresses. Both problems apply a normal stress of 6,000 psi at the top of the grid, while Problem 1 enforces zero normal displacements at the four vertical faces of the grid, and Problem 2 applies a normal stress of 4,000 psi at these same faces. Assuming uniaxial strain behavior for Problem 1 and constant total stresses for Problem 2, the explicitly coupled simulations in this paper use constant values of 3.71×10^{-4} psi^{-1} and 6.00×10^{-4} psi^{-1} for the compressibility in Eq. 4. The fluid and porous solid start in equilibrium in both problems, with minimal fluid motion and initial strains of less than 0.03%.

A vertical well with a wellbore radius of 0.25 ft is completed in the center of the pattern in all 10 layers of the grid, cells (6,6,1–10). The well is produced at a rate of 15,000 B/D for 500 days with

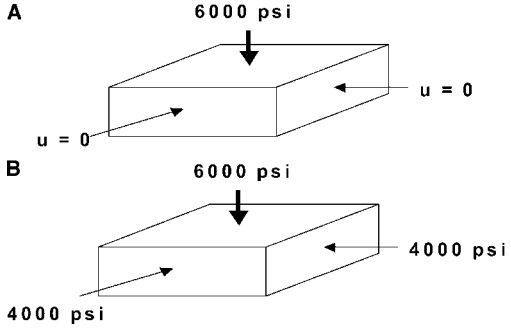

Fig. 1—(a) Constrained displacements for Problem 1. (b) Unconstrained displacements for Problem 2.

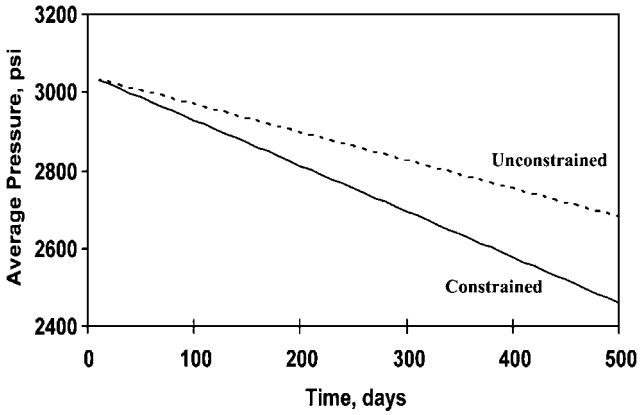

Fig. 2—Average pressures for Problems 1 and 2.

a timestep size of 10 days. No flow boundary conditions are assumed for the fluid at all faces of the grid.

Fig. 2 shows average pore-volume-weighted reservoir pressures for Problems 1 and 2 using the three different techniques. All techniques produce nearly identical results for each problem. Fig. 2 shows how geomechanical stress or displacement boundary conditions influence the pressure response in the reservoir. Problem 2 shows much less pressure drop than Problem 1 because of the support provided by the constant stress boundary conditions on the sides of the reservoir. This support is evident in the values of the horizontal stresses at the vertical faces of the reservoir. At the end of the simulation, the normal stress at the center of each vertical face is 3,650 psi for Problem 1 and 4,000 psi for Problem 2. For Problem 1, the sides of the reservoir are constrained and the compressive horizontal stresses at the vertical faces decrease as the porous solid attempts to contract caused by fluid depletion. For Problem 2, the sides of the reservoir are free to move and a constant compressive stress is applied at each vertical face.

The runtime information for Problems 1 and 2 are displayed in **Tables 1 and 2.** The column for iterations is the number of nonlinear iterations during a simulation. The explicitly coupled technique is faster than the other two techniques for this problem because it performs a small number of updates for the displacements when using an E_{rel} tolerance of 0.001. The explicitly coupled technique performs 19 and 16 updates for the displacements for Problems 1 and 2, respectively.

Fig. 3 shows the subsidence at the top of the reservoir at the well for Problems 1 and 2. The two problems produce similar displacements at early times, but the problems deviate substantially at later times. The change in subsidence in Fig. 3 is not a linear function of the average pressure drop in Fig. 2 until later in the run, when a pseudosteady state is reached for the pressure behavior.

The total subsidence for Problem 1 is 12.2 ft after 500 days. This corresponds to an average vertical strain of 6.1%, which is very large considering that the calculations are based upon infinitesimal strain assumptions. Even though the pressures in Fig. 2 are based upon calculations using infinitesimal strains, it is expected that the results should not change substantially if the calculations are repeated using a finite-strain formulation. Based upon a simple uniaxial strain analysis, a finite-strain simulation should predict a final average pressure for the constrained case that is approximately 10 psi larger than the result shown in Fig. 2.

The explicitly coupled technique performed 19 updates for displacements for Problem 1, where the program selected the update

TABLE 2—RUNTIME INFORMATION FOR PROBLEM 2

Technique	CPU Time	Timesteps	Iterations
Explicit	7.8 seconds	50	52
Iterative	10.7	50	52
Full	12.4	50	51

TABLE 1—RUNTIME INFORMATION FOR PROBLEM 1

Technique	CPU Time	Timesteps	Iterations
Explicit	8.0 seconds	50	52
Iterative	10.7	50	51
Full	13.3	50	51

times based upon using $E_{rel} \approx \beta(\Delta V_p)_{rel}$ to estimate the relative error between the pressure-calculated pore volume, Eq. 4, and the strain-calculated pore volume, Eq. 2. However, as noted earlier, the true error in E_{rel} is normally only available at the selected update times. The program was modified to calculate the true error in E_{rel} at all times in order to show the values of E_{rel} for those times when no actual updates were performed for displacements. The values of E_{rel} for Problem 1 are shown in **Fig. 4** for all timesteps. The update tolerance for the run was $E_{rel} = 0.001$. The actual error was above this value for all times before 100 days, so the program updated displacements for every step prior to 100 days. Currently, the program uses E_{rel} to determine when updates should be performed for timesteps, but the results in Fig. 4 for early times suggest that E_{rel} could also be useful for timestep selection or for switching to an iteratively coupled technique. Displacements were printed every 100 days, so the program updated displacements at each print time. In Fig. 4, one can see a drop in E_{rel} each time that displacement updates are performed.

Problem 3. Problem 3 is modeled after a problem presented by Gutierrez and Lewis (1998). Problem 3 includes a soft productive reservoir that is contained within a stiff nonpay region as shown in **Fig. 5.** Problem 3 displays a geomechanical effect at the boundary of the reservoir that cannot be seen in reservoir simulations that do not include geomechanical calculations. For this problem, geomechanical effects cause the fluid pressures to increase at the boundary of the reservoir during the initial stages of depletion.

The grid is 21×21×12 and includes both the reservoir and nonpay regions. Gridblock lengths in the *x*-direction are 4,000 ft each for the first 5 gridblocks, 2,000 ft each for the next 11 gridblocks, and 4,000 ft each for the last 5 gridblocks. Gridblock lengths in the *y*-direction are half the corresponding values in the *x*-direction. The top of the grid is at a depth of 0 ft, and the thicknesses in the vertical direction are 4,000, 3,000, 2,000, 800, and 200 ft for the first five layers that represent the overburden. The next five layers have thicknesses of 50 ft each and represent the reservoir. The last two layers have thicknesses of 100 ft each and represent the underburden. The horizontal and vertical permeabilities are 100 and 10 md, respectively, in the reservoir, cells (6-16,6-16,6-10). Permeabilities are zero in the nonpay region. The initial in-situ porosity is 25% in both the reservoir and nonpay regions.

The fluid is single-phase, with a formation volume factor of 1 at 14.7 psi, a viscosity of 1 cp, a fluid density of 62.4 lbm/ft^3 at

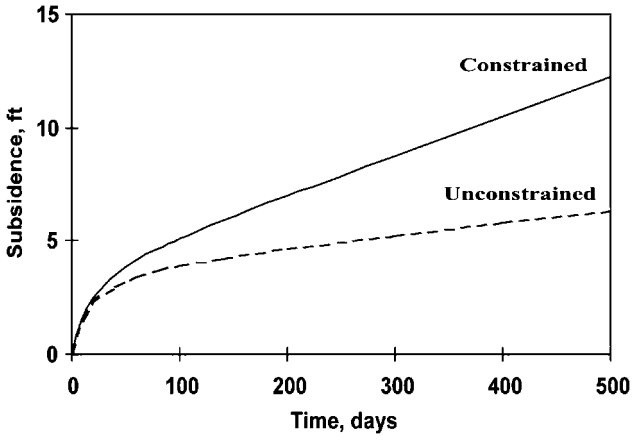

Fig. 3—Subsidence for Problems 1 and 2.

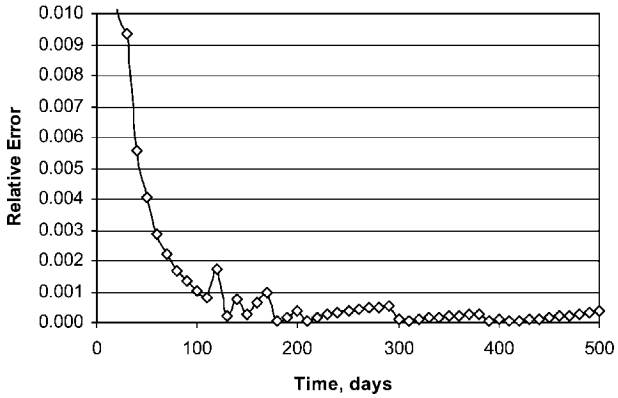

Fig. 4—Relative pore volume error for Problem 1.

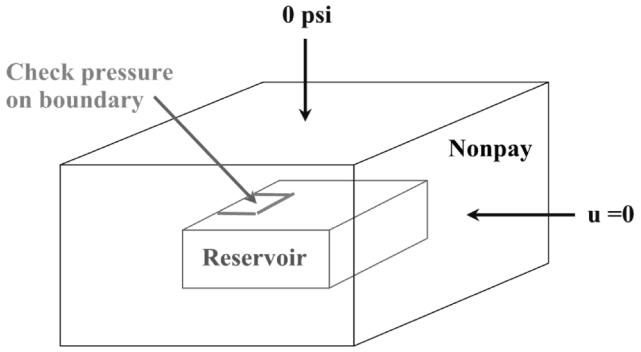

Fig. 5—Reservoir and nonpay regions for Problem 3.

14.7 psi, and fluid compressibility of 3×10^{-6} psi^{-1}. A nonzero fluid compressibility is used for this problem because a zero fluid compressibility makes the porous solid incompressible in the nonpay region. The initial fluid pressure is 14.7 psi at the surface with a hydrostatic gradient of 0.437 psi/ft.

The elastic moduli are 1×10^4 psi in the reservoir and 1×10^6 psi in the nonpay region, Poisson's ratio is 0.25 everywhere, and the initial in-situ solid density (solid material without pores) is 2.7 g/cm^3. The initial vertical stress is 0 psi at the surface with a vertical stress gradient of 0.9869 psi/ft throughout the grid, and initial horizontal stresses are equal to half of the vertical stress. The bottom and sides of the grid have zero normal displacement constraints, and all faces of the grid have zero tangential stresses. Assuming uniaxial strain behavior for this problem, the explicitly coupled simulation uses values of 3.33×10^{-4} psi^{-1} and 3.33×10^{-6} psi^{-1} for the compressibility in Eq. 4 in the reservoir and nonpay regions, respectively. The reservoir starts out in equilibrium with maximum strains of less than .002%.

A vertical well with a wellbore radius of 0.25 ft is completed in the center of the reservoir in all five layers, cells (11,11,6-10). The well is produced at a rate of 50,000 STB/D for 4,000 days with a timestep size of 20 days for the first 400 days, followed by timesteps of 200 days, stopping at 4,000 days. Smaller timesteps are taken at the beginning of the run to produce an accurate solution for the pressure increase at the reservoir boundary. Iteratively coupled and fully coupled techniques should be able to produce accurate results using the timesteps specified for this problem, but explicitly coupled techniques may require timesteps that are smaller than 20 days because of time-discretization errors that arise because of the explicit coupling.

Fig. 6 shows average pore-volume-weighted pressures in the reservoir (excluding nonpay region) using the three different techniques. The three techniques produce significantly different results in Fig. 6 after the timestep size increases from 20 to 200 days. The three techniques also predict large differences in pressures at the boundary of the reservoir at early times.

It is clear from Fig. 6 that Eq. 4 produces poor estimates of the pore-volume changes for this problem when one uses the explicitly coupled technique with 20- and 200-day timesteps even though the displacements are updated each timestep. The values of E_{rel} for the explicitly coupled technique are shown in **Fig. 7.** The update tolerance for the run was $E_{rel}=0.001$, and one can see that the errors exceeded the tolerance by a large amount.

In order to produce reasonable results for the iteratively coupled and explicitly coupled techniques, the iteratively coupled technique requires a tighter tolerance on the nonlinear iterations and the explicitly coupled technique requires smaller timesteps. The runs were repeated for the iteratively coupled technique using a nonlinear volume error tolerance of 0.0001 and for the explicitly coupled technique using a timestep size of 1 day. One can improve the explicitly coupled results by using a smaller value of estimated compressibility for this problem; however, values that are too small will produce oscillations in well pressures. **Fig. 8** shows E_{rel} for the explicitly coupled technique when using constant 1-day timesteps. In Fig. 8, it appears that the explicitly coupled technique would produce more accurate and faster results if the timesteps were smaller than 1 day early in the run and larger than 1 day later in the run. This goes back to the earlier suggestion that E_{rel} may be a useful measure to control the timestep for the explicitly coupled technique.

Fig. 9 shows the subsidence at the top of the reservoir and at the surface for all three techniques. The explicitly coupled results included in Fig. 9 use a timestep size of 1 day for the simulation. The original explicitly coupled results using timestep sizes of 20 and 200 days did not agree well with the results in Fig. 9 predicting a final subsidence of 6.47 ft at the top of the reservoir. The final subsidence in Fig. 9 at the top of the reservoir is 7.76 ft.

Fig. 10 shows the pressure behavior at the boundary of the reservoir in cell (6,11,6). Initially, the reservoir pressure increases as the reservoir is depleted, because some of the vertical load that was supported at the center of the reservoir is transferred to the edges of the reservoir. The amount of pressure increase at the edge of the reservoir is a strong function of the contrast in elastic moduli between the reservoir and nonpay regions. This pressure increase

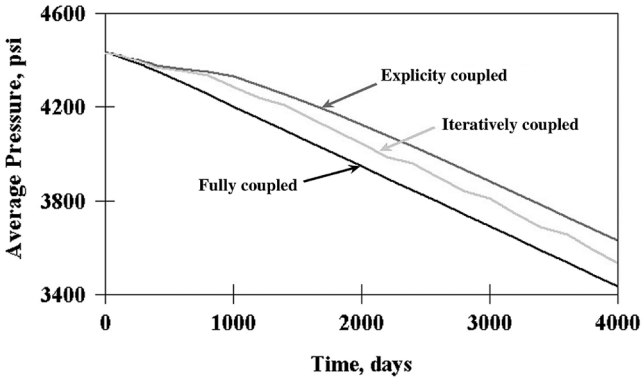

Fig. 6—Average reservoir pressures for Problem 3.

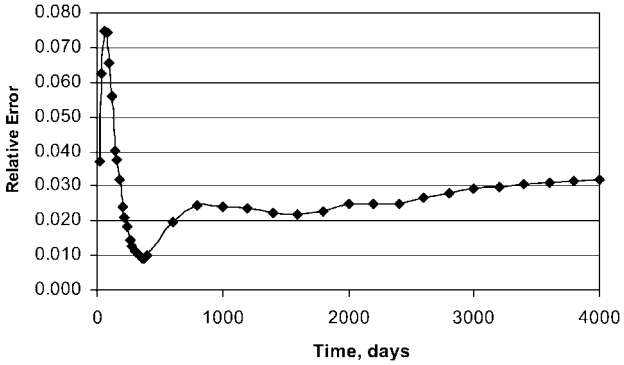

Fig. 7—Relative pore volume error with 20- and 200-day steps.

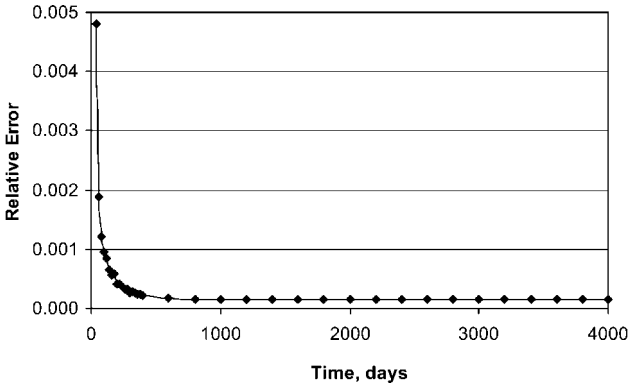

Fig. 8—Relative pore volume error with 1-day steps.

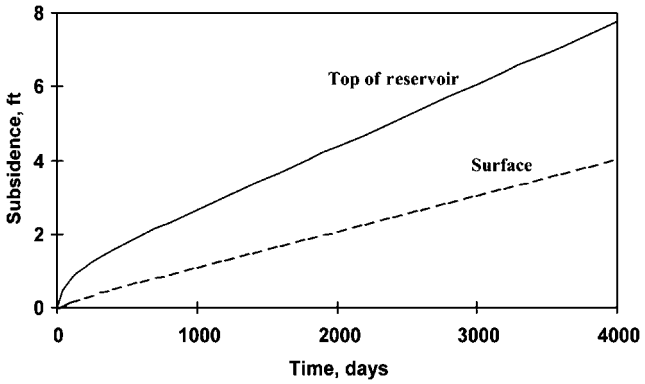

Fig. 9—Subsidence for problem 3.

cannot be observed in a reservoir depletion problem that does not include geomechanical calculations. The iteratively coupled results in Fig. 10 use a volume error tolerance of 0.0001, and the explicitly coupled results use a timestep size of 1 day, updating displacements every timestep. The deviation of the explicitly coupled results from the iteratively coupled and fully coupled results in Fig. 10 is probably caused by the errors in E_{rel} that occur at early times in Fig. 8.

The runtime results for Problem 3 are shown in **Table 3.** The explicitly coupled technique is much slower than the other two techniques for this problem, because it requires much smaller timestep sizes. The fully coupled and iteratively coupled techniques also exhibit time discretization errors, but time discretization errors play a much larger role for the explicitly coupled technique. The iteratively coupled technique is slower than the fully coupled technique, because the iteratively coupled technique requires a large number of nonlinear iterations for convergence. Also, the iteratively coupled technique exhibits only a first-order rate of convergence for the nonlinear iterations because of the sequential nature of updating the flow and displacement equations.

Problem 4. Problem 4 is a three-phase quarter of a five-spot pattern with a water-injection well in one corner of the grid and a production well in the diagonally opposite corner of the grid. The production rate is larger than the injection rate, so the reservoir pressure decreases throughout the simulation.

The grid for Problem 4 is displayed in **Fig. 11,** showing water saturations at the end of 25 years. The grid is 21×21×11 with $\Delta x = \Delta y = 60$ ft in the horizontal directions and $\Delta z = 20$ ft in the vertical direction. The top of the grid is at a depth of 4,000 ft, and the initial in-situ reservoir porosity is 30%. Reservoir permeabilities vary by layer with horizontal permeabilities equal to 5, 100, 20, 20, 20, 100, 20, 20, 100, 20, and 20 md, respectively. Vertical permeabilities are 0.01 times horizontal permeabilities. Two-phase relative permeabilities and capillary pressures are listed in **Tables 4 and 5,** and Stone 2 is used for three-phase relative permeabilities (Stone 1973).

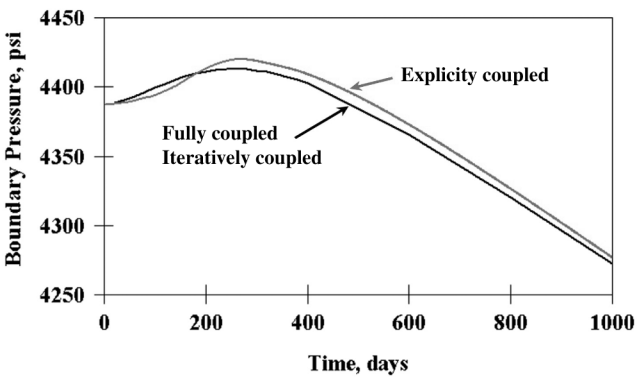

Fig. 10—Pressure at boundary of reservoir for Problem 3.

Water has a formation volume factor of 1 at 14.7 psi, a viscosity of 1 cp, a fluid density of 62.4 lbm/ft^3 at 14.7 psi, and fluid compressibility of 3×10^{-6} psi^{-1}. The oil and gas densities at the surface are 56.0 lbm/ft^3 and 57.0 lbm/mcf, respectively. Pressure-dependent oil and gas properties are listed in **Table 6.**

The initial reservoir pressure is in hydrostatic equilibrium with a fluid pressure of 3,010 psi at 4,010 ft, and the initial fluid saturations are constant and are 20, 80, and 0% for water, oil, and gas, respectively. The oil is initially undersaturated with a bubblepoint pressure of 3000 psi and an oil compressibility of 10^{-5} psi^{-1} in all layers.

The elastic modulus is 5×10^4 psi, Poisson's ratio is 0.35, and the initial in-situ solid density (solid material without pores) is 2.7 g/cm^3. The initial vertical stress is 4,000 psi at the top of the reservoir, with a vertical stress gradient of 0.9256 psi/ft throughout the grid, and initial horizontal stresses are equal to half of the vertical stress. The bottom and sides of the grid have zero normal displacement constraints and all faces of the grid have zero tangential stresses. Assuming uniaxial strain behavior for this problem, the explicitly coupled simulation uses a value of 4.15×10^{-5} psi^{-1} for compressibility in Eq. 4.

Vertical wells are completed in diagonally opposite corners of the grid in all 11 layers. The water injector has a prescribed rate of 500 STB/D (¼ of the well's total rate), and the production well has a prescribed liquid rate of 750 STB/D (¼ of the well's total rate) with a limiting bottomhole pressure of 500 psi. Wellbore radii of 0.069 ft (instead of 0.25 ft) are used to represent wells of radii 0.25 ft that are at the corners of the gridblocks (Kuniansky and Hillestad 1980) and a multiplying factor of 0.25 is used for the wellbore constants because only ¼ of a well's production is being simulated in the pattern. Simulations are performed for 25 years using timestep sizes that are controlled by stability considerations for the IMPEM technique.

The three techniques produce nearly identical results for problem 4. **Fig. 12** shows average pore-volume-weighted, oil-phase pressures and subsidence in the center of the pattern at the top of the reservoir. **Fig. 13** shows the wellbore pressure, gas/oil ratio, and water/oil ratio at the production well.

The runtime information for Problem 4 is displayed in **Table 7.** The explicitly coupled technique is much faster than the other two techniques for this problem because it performs a small number of geomechanical updates during the simulation. The explicitly coupled technique requires only 33 updates for displacements throughout the simulation. A minimum of 25 updates are required because displacements are printed each year during the simulation.

TABLE 3—RUNTIME INFORMATION FOR PROBLEM 3

Technique	CPU Time	Timesteps	Iterations
Explicit	51.8 minutes	4,000	4,000
Iterative	6.9	38	449
Full	4.3	38	38

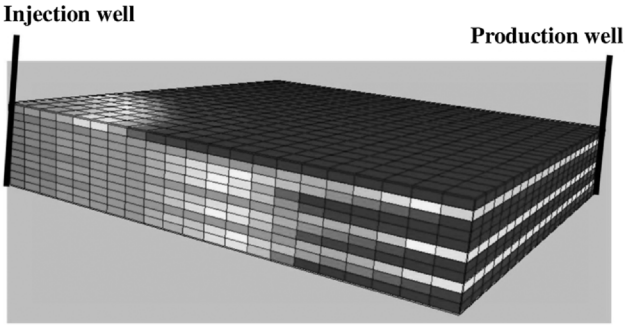

Fig. 11—Water saturations after 25 years for Problem 4.

The iteratively coupled and fully coupled techniques would perform better for this problem if they were combined with the implicit timestepping option in the program, rather than with the IMPEM option, but it is expected that the explicitly coupled option would still be the best option because few geomechanical updates are required.

A run was performed without geomechanical calculations using a value of 4.15×10^{-5} psi^{-1} for c_r in Eq. 1, and the results reproduced the pressure and fluid histories in Figs. 12 and 13. The simulation without geomechanical calculations took 7.2 minutes; therefore, for this problem, geomechanical calculations add only 25% to the overall computational time for the model when using the explicitly coupled technique.

Conclusions

Explicitly coupled, iteratively coupled, and fully coupled techniques have been applied to four sample problems. The three techniques produce nearly identical results on Problems 1, 2, and 4 using the same timestep sizes and the same convergence tolerances. Problem 3 involves geomechanical effects that are not present in the other three problems and the three techniques initially produced different results for this problem; however, all three techniques produced similar results when a tight tolerance was used for the nonlinear iterations for the iteratively coupled technique and when small timesteps were used for the explicitly coupled technique. All problems in this paper are described in detail so that the results presented here may be used for comparison with other geomechanical/porous-flow simulators.

TABLE 5—GAS/OIL DATA FOR PROBLEM 4

S_w+S_o	K_{rog}	K_{rg}	P_{gc}
0.2	0.0	0.6303	3.2
0.25	0.0	0.5511	2.8
0.3	0.0	0.4772	2.5
0.35	0.0026	0.4086	2.1
0.4	0.0104	0.3454	1.8
0.45	0.0234	0.2874	1.5
0.5	0.0416	0.2348	1.3
0.55	0.0651	0.1875	1.0
0.6	0.0937	0.1455	0.8
0.65	0.1275	0.1089	0.6
0.7	0.1666	0.0775	0.5
0.75	0.2108	0.0514	0.3
0.8	0.2709	0.0307	0.2
0.85	0.3149	0.0153	0.1
0.9	0.3748	0.0052	0.0
0.95	0.4398	0.0004	0.0
0.97	0.4673	0.0	0.0
1.0	0.5102	0.0	0.0

TABLE 4—WATER/OIL DATA FOR PROBLEM 4

S_w	K_{rw}	K_{row}	P_{wc}
0.2	0.0	0.5102	6.4
0.25	0.0039	0.4133	5.6
0.3	0.0156	0.3266	4.9
0.35	0.0352	0.2500	4.2
0.4	0.0625	0.1837	3.6
0.45	0.0977	0.1276	3.0
0.5	0.1406	0.0816	2.5
0.55	0.1914	0.0459	2.0
0.6	0.2500	0.0204	1.6
0.65	0.3164	0.0051	1.2
0.7	0.3906	0.0	0.9
0.8	0.5625	0.0	0.4
0.9	0.7656	0.0	0.1
1.0	1.0	0.0	0.0

The three coupling techniques produce similar results, and one's selection of a technique is determined by ease of implementation, program availability, numerical stability, and computational efficiency. No single technique worked best on all four problems presented in this paper. The fully coupled technique worked best for Problem 3, running 12 times faster than the explicitly coupled technique; and the explicitly coupled technique worked best for Problem 4, running five times faster than the fully coupled technique.

Nomenclature

c_r = reservoir compressibility, Lt^2/m, psi^{-1}
E = elastic modulus, m/Lt^2, psi
E_{rel} = relative difference in pore volumes
M = Biot's poroelastic parameter, m/Lt^2, psi
p = fluid pressure, m/Lt^2, psi
p_o = initial fluid pressure, m/Lt^2, psi
V_p = pore volume, L^3, ft^3
$\tilde{V}_p$ = pore volume estimate from pressure equation, L^3, ft^3
V_b^o = initial grid block volume, L^3, ft^3
V_p^o = initial pore volume, L^3, ft^3
α = Biot's poroelastic parameter, dimensionless
δ_{ij} = Kronecker delta, dimensionless

TABLE 6—PRESSURE-DEPENDENT OIL AND GAS DATA FOR PROBLEM 4

Pressure (psi)	B_o (rvb/STB)	B_g (rvb/mcf)	R_s (mcf/STB)	μ_o (cp)	μ_g (cp)
300.00	1.0663	10.2582	.0610	1.5	.02
600.00	1.0931	4.9878	.1161	1.5	.02
900.00	1.1173	3.2461	.1681	1.5	.02
1200.00	1.1408	2.3855	.2197	1.5	.02
1600.00	1.1718	1.7522	.2894	1.5	.02
2000.00	1.2030	1.3838	.3608	1.5	.02
2400.00	1.2346	1.1479	.4342	1.5	.02
2800.00	1.2667	.9876	.5102	1.5	.02
3000.00	1.2843	.9221	.5521	1.5	.02
3200.00	1.2996	.8743	.5889	1.5	.02
3600.00	1.3334	.7921	.6708	1.5	.02
4000.00	1.3683	.7312	.7561	1.5	.02
4500.00	1.4137	.6763	.8685	1.5	.02

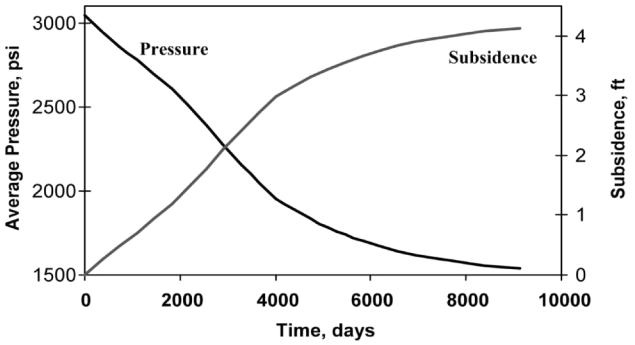

Fig. 12—Average pressure and subsidence for Problem 4.

Δ = change in a variable, dimensionless
ε_{ij} = strain, expansion is positive, dimensionless
ε_{kk} = volumetric strain, dimensionless
λ = Lame constant, m/Lt^2, psi
μ = Lame constant, m/Lt^2, psi
ν = Poisson's ratio, dimensionless
σ_{ij} = total stress, tension is positive, m/Lt^2, psi
σ^o_{ij} = initial total stress, m/Lt^2, psi
φ_o = initial porosity, dimensionless

Acknowledgments

BP plc provided a copy of ACRES to the U. of Texas at Austin for running the comparisons in this paper. The authors would like to acknowledge the support of the U.S. Dept. of Energy (DOE), NSF, NGOTP, and the Industrial Affiliates of the Center for Subsurface Modeling at the U. of Texas at Austin. Sandia is a multiprogram laboratory operated by Sandia Corp., a Lockheed Martin company, for the DOE under contract DE-AC04-94AL85000.

References

ARCO Reservoir Simulator Development: "Appendix 30: Poroelastic Calculations," ACRES Reference Manual, Internal ARCO Document, ARCO, Plano, Texas (1999).

Belylschko, T., Ong, J.S.J., Liu, W.K., and Kennedy, J.M.: "Hourglass Control in Linear and Nonlinear Problems," *Comp. Methods in Applied Mech. and Eng.* (1984) **43,** 251.

Biot, M.A.: "General Solutions of the Equations of Elasticity and Consolidation for a Porous Material," *Journal of Applied Mechanics* (1956) **23,** 91.

Fung, L.S.K., Buchanan, L., and Wan, R.G.: "Coupled Geomechanical-Thermal Simulation for Deforming Heavy-Oil Reservoirs," *J. Cdn. Pet. Tech.* (1994) **33,** No. 4, 22.

Gutierrez, M. and Lewis, R.W.: "The Role of Geomechanics in Reservoir Simulation," paper SPE/ISRM 47392 presented at the 1998 SPE/ISRM Rock Mechanics in Petroleum Engineering Conference, Trondheim, July 8–10.

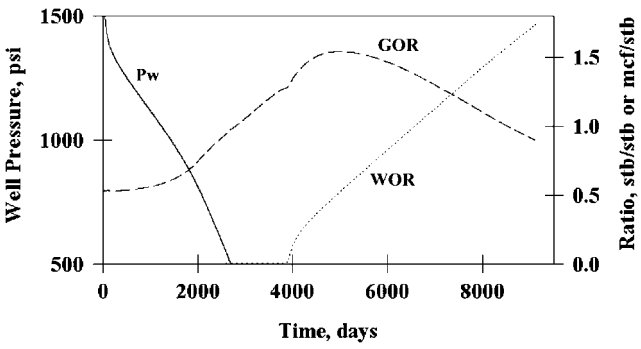

Fig. 13—Production history for Problem 4.

TABLE 7—RUNTIME INFORMATION FOR PROBLEM 4

Technique	CPU Time	Timesteps	Iterations
Explicit	9.0 minutes	3,324	3,325
Iterative	40.6	3,326	3,326
Full	47.5	3,326	3,326

Kosloff, D. and Frazier, G.A.: "Treatment of Hourglass Patterns in Low Order Finite Element Codes," *Intl. J. for Num. and Anal. Methods in Geomechanics* (1978) **2,** 57.

Kuniansky, J. and Hillestad, J.G.: "Reservoir Simulation Using Bottom-hole Pressure Boundary Conditions," *SPEJ* (1980) **20,** No. 6, 473.

Lewis, R.W. and Sukirman, Y.: "Finite Element Modelling of Three-Phase Flow in Deforming Saturated Oil Reservoirs," *Intl. J. for Num. and Anal. Methods in Geomech.* (1993) **17,** 577.

Li, X. and Zienkiewicz, O.C.: "Multiphase Flow in Deforming Porous Media and Finite Element Solutions," *Computers and Structures* (1992) **45,** 211.

Maenchen, G. and Sack, S.: "The Tensor Code," *Methods of Comp. Physics,* Academic Press, New York City (1964) **3,** 181–210.

Minkoff, S.E., Stone, C.M., Arguello, J.G., Bryant, S., Eaton, J., Peszynska, M., and Wheeler, M.: "Staggered in Time Coupling of Reservoir Flow Simulation and Geomechanical Deformation: Step 1—One-Way Coupling," paper SPE 51920 presented at the 1999 SPE Reservoir Simulation Symposium, Houston, 14–17 February.

Minkoff, S., Stone, C., Arguello, J., Bryant, S., Eaton, J., Peszynska, M., and Wheeler, M.: "Coupled Geomechanics and Flow Simulation for Time-Lapse Seismic Modeling," paper presented at the 1999 Annual International Meeting of the Society of Exploration Geophysicists, Houston.

Minkoff, S., Stone, C., Bryant, S., Peszynska, M., and Wheeler, M.: "Coupled Fluid Flow and Geomechanical Deformation Modeling'," *J. of Petroleum Science and Eng.* (2003) **38,** 37.

Settari, A. and Mourits, F.M.: "Coupling of geomechanics and reservoir simulation models," *Comp. Methods and Advances in Geomech.,* Siriwardane and Zeman (eds.), Balkema, Rotterdam (1994) 2151–2158.

Settari, A. and Walters, D.A.: "Advances in Coupled Geomechanical and Reservoir Modeling With Applications to Reservoir Compaction," paper SPE 51927 presented at the 1999 SPE Reservoir Simulation Symposium, Houston, 14–17 February.

Stone, H.L.: "Estimation of Three-Phase Relative Permeability and Residual Oil Data," *J. Can. Pet. Tech.* (1973) **12,** 53.

Tortike, W.S. and Farouq Ali, S.M.: "A Framework for Multiphase Nonisothermal Fluid Flow in a Deforming Heavy Oil Reservoir," paper SPE 16030 presented at the 1987 SPE Symposium on Reservoir Simulation, San Antonio, Texas, 1–4 February.

SI Metric Conversion Factors

bbl × 1.589 874	E–01	= m^3
cp × 1.0*	E-03	= Pa s
ft × 3.048*	E–01	= m
lbm × 4.535924	E–01	= kg
mcf × 2.831 685	E+01	= m^3
md × 9.869 233	E–04	= μm^2
psi × 6.894 757	E+00	= kPa
psi^{-1} × 1.450 377	E–01	= kPa^{-1}

*Conversion factors are exact.

Rick H. Dean is President of Simwulf Systems in Plano, Texas. He has specialized in reservoir simulation and engineering mechanics as a Senior Research Associate at the U. of Texas at Austin, as a Senior Research Advisor at ARCO Oil and Gas, and as an assistant professor in engineering mechanics at the Ohio State U. Dean holds a BA degree from Earlham College and MA and PhD degrees from Harvard U. **Xiuli Gai** is a post-

doctoral fellow in the Center for Subsurface Modeling at the U. of Texas at Austin. Her research interests are in the development of mathematical and computational methods for large-scale reservoir simulation coupled with geomechanics. Gai holds a PhD degree in petroleum engineering from the U. of Texas at Austin and an MS degree in reservoir geology from Daqing Petroleum Inst., China. **Charles M. (Mike) Stone** is a Principal Member of the Technical Staff at Sandia Natl. Laboratories in Albuquerque, New Mexico. He does research in the development of computational methods for a wide variety of engineering applications. He has authored papers in the areas of drillstring dynamics, stress analysis of PDC bits, and coupled geomechanics and reservoir simulation. Stone holds an MS degree from the U. of Texas at Austin. **Susan E. Minkoff** is an assistant professor in the Dept of Mathematics and Statistics at the U. of Maryland, Baltimore County. Her thesis work was on source estimation for seismic inverse problems. Her postdoctoral work at the U. of Texas involved upscaling for reservoir flow simulation. After leaving the U. of Texas, she worked in multiphysics simulation at Sandia Natl. Labs. At UMBC she has been working on faster wave-equation solvers for inversion of the deep crust, polarization mode dispersion compensation for optical communications, and modeling of carbon dioxide leakage from underground storage sites. She holds a BS degree from Duke U. and a PhD degree from Rice U. in computational and applied mathematics.